

Virus-induced activation of the rac1 protein at the site of respiratory syncytial virus assembly is a requirement for virus particle assembly on infected cells

Laxmi Iyer Ravi^a, Timothy J. Tan^a, Boon Huan Tan^{a,b,c}, Richard J. Sugrue^{a,*}

^a School of Biological Sciences, Nanyang Technological University, 60 Nanyang Drive, 637551, Singapore

^b Defense Medical and Environment Research Institute, DSO National Laboratories, 27 Medical Drive, 117510, Singapore

^c Infection and Immunity, Lee Kong Chian School of Medicine, Nanyang Technological University, 11 Mandalay Road, Singapore, 308232, Singapore

ARTICLE INFO

Keywords:

Respiratory syncytial virus
Virus assembly
rac1 protein
F-actin
virus-like particles

ABSTRACT

The distributions of the rac1, rhoA and cdc42 proteins in respiratory syncytial virus (RSV) infected cells was examined. All three rhoGTPases were detected within inclusion bodies, and while the rhoA and rac1 proteins were associated with virus filaments, only the rac1 protein was localised throughout the virus filaments. RSV infection led to increased rac1 protein activation, and using the rac1 protein inhibitor NS23766 we provided evidence that the increased rac1 activation occurred at the site of RSV assembly and facilitated F-actin remodeling during virus morphogenesis. A non-infectious virus-like particle (VLP) assay showed that the RSV VLPs formed in lipid-raft microdomains containing the rac1 protein, together with F-actin and filamin-1 (cell proteins associated with virus filaments). This provided evidence that the virus envelope proteins are trafficked to membrane microdomains containing the rac1 protein. Collectively, these data provide evidence that the rac1 protein plays a direct role in the RSV assembly process.

1. Introduction

Mature respiratory syncytial virus (RSV) particles are surrounded by a lipid envelope, in which the virus fusion (F) and attachment (G) proteins are inserted. The F protein mediates fusion of the virus and host cell membranes during virus entry, and a primary role for the G protein in virus attachment to susceptible cells has been demonstrated (Levine et al., 1987). The virus polymerase complex forms part of a larger ribonucleoprotein (RNP) complex, which is formed by the interaction between the viral genomic RNA (vRNA), the nucleocapsid (N) protein, the phosphoprotein (P protein), the M2-1 protein and the large (L) protein (Collins et al., 1996; Grosfeld et al., 1995; Yu et al., 1995). Two distinct virus structures are formed in RSV-infected epithelial cells, which are referred to as virus filaments and inclusion bodies. The virus RNP complex is packaged within the virus filaments, which assemble on the apical cell surface of infected cells as filamentous projections that are approximately 200 nm thick and up to 6 μm in length (Roberts et al., 1995). During the course of infection the virus filaments remain largely cell-associated, and mediate localized virus transmission in cell monolayers (Huong et al., 2016). The inclusion bodies are large structures that

form in the cytoplasm of RSV-infected cells, and these are locations in the cell where the virus polymerase-associated proteins and virus-specific RNA accumulate (Carromeu et al., 2007; Garcia-Beato and Melero, 2000; Garcia et al., 1993; Santangelo et al., 2006). The cellular processes that lead to the assembly of mature RSV filaments are still not fully understood, but evidence suggests that this process is mediated by a combination of viral and cellular factors.

Virus assembly occurs at specific locations on the cell surface, and the virus structural proteins are subsequently incorporated into the developing virus filaments (Jeffree et al., 2003). It is proposed that these locations also contain a variety of essential cellular factors that are required to facilitate virus assembly (Jeffree et al., 2003) (Radhakrishnan et al., 2010). For example, the involvement of lipid-raft microdomains in RSV morphogenesis has been demonstrated (Brown et al., 2002b; McCurdy and Graham, 2003), and available evidence indicates the involvement of specialized types of lipid raft microdomains called caveolae (Brown et al., 2002a; Ludwig et al., 2017). This suggests that RSV assembly process occurs within a unique cellular environment at the cell surface, which may be analogous to the budzone that has been described for the site of influenza virus assembly (Leser and Lamb, 2017;

* Corresponding author.

E-mail address: rjsugrue@ntu.edu.sg (R.J. Sugrue).

<https://doi.org/10.1016/j.virol.2021.02.008>

Received 7 August 2020; Received in revised form 17 December 2020; Accepted 16 February 2021

Available online 22 February 2021

0042-6822/© 2021 Elsevier Inc. This article is made available under the Elsevier license (<http://www.elsevier.com/open-access/userlicense/1.0/>).

Schmitt and Lamb, 2005). In this context, a role for actin in RSV morphogenesis has been demonstrated (Bitko et al., 2003; Burke et al., 1998; Jeffree et al., 2007; Kallewaard et al., 2005), and several studies have proposed that an actin-based motility mechanism mediates RSV transmission (Ravi et al., 2013; Ulloa et al., 1998). Interestingly, changes in filamentous actin (F-actin) structure coincides with the formation of RSV particles, and actin and other cellular proteins that play a role in the

maintenance of F-actin structure are also present in the virus filaments (Radhakrishnan et al., 2010). This has suggested that localized reorganization of F-actin structures at the site of RSV assembly may facilitate the process of virus assembly. Members of the rho family of GTPases have been shown to regulate many aspects of intracellular actin dynamics, and the rhoA, cdc42 and rac1 proteins are among the most widely researched and the best understood members of this family of

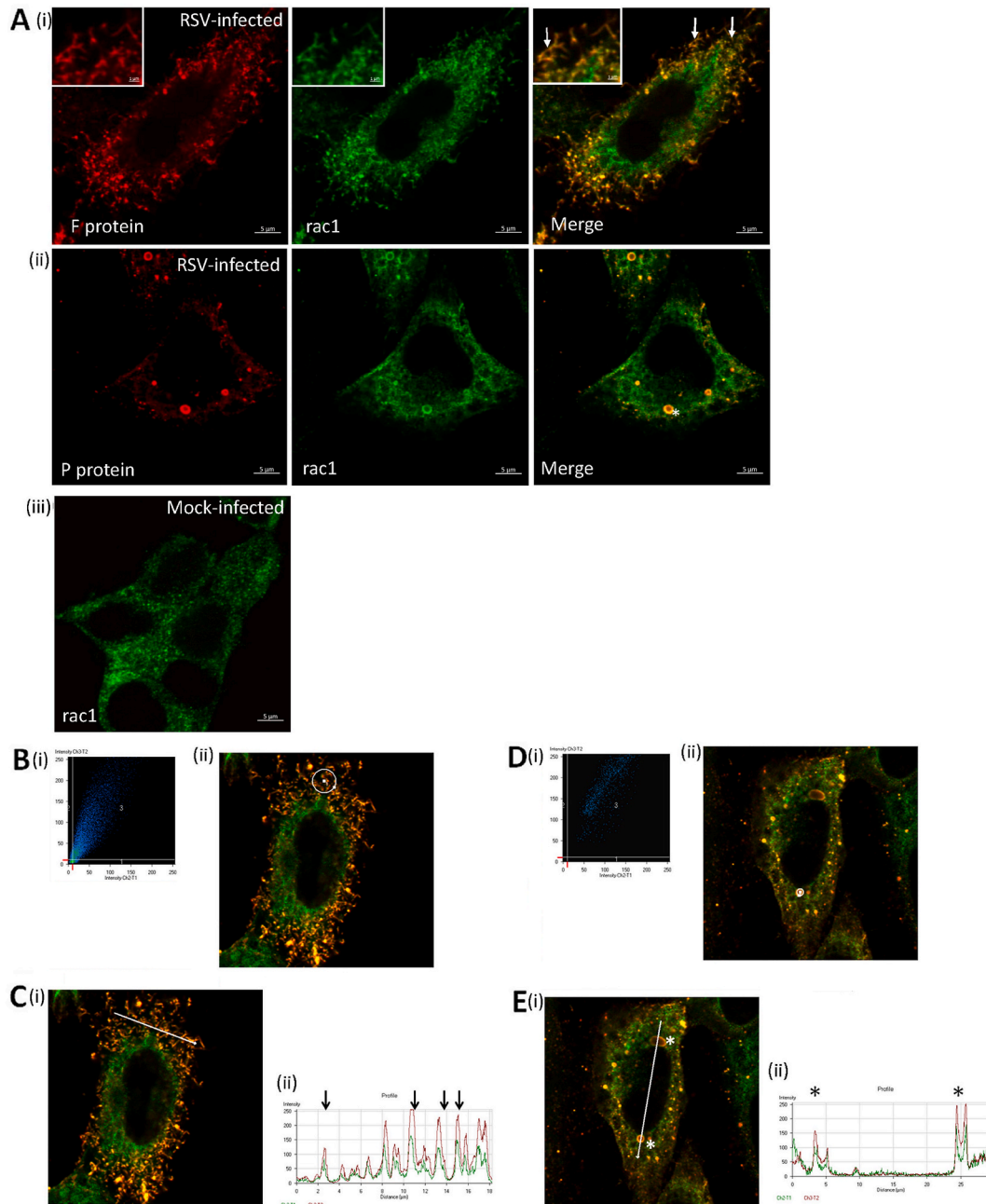


Fig. 1. The distribution of the rac1 protein in RSV-infected cells. HEp2 cells were RSV-infected and at 18 h post-infection (hpi) the cells were co-stained with (A) (i) anti-rac1 and anti-F, and (ii) anti-rac1 and anti-P. The cells were visualized using confocal microscopy at a focal plane that allowed (i) virus filament detection (highlight by white arrows) and (ii) inclusion body detection (highlighted by *). Enlarged image of area highlighted by white boxes are shown in plate (i). (iii) Also shown are mock-infected cells stained with anti-rac1. (B) (i) The scatter-plot of the red and green pixels in the anti-rac1 (green) and anti-F (red) co-stained virus filaments in (ii) the area (highlighted by the white circle) where the pixels were sampled (Pearson's correlation coefficient $R = 0.88$; Mander's overlap coefficient = 0.91). (C) The intensity of the anti-rac1 (green) and anti-F (red) staining across the infected cell at an optical plane where the virus filaments were visualized. Cross-section analysis indicated by white line in (i) and (ii) plotted as an intensity map. Individual virus filaments are highlighted (black arrow). (D) (i) The scatter-plot of the red and green pixels in the anti-rac1 (green) and anti-P (red) co-stained virus inclusion bodies in (ii) the area (highlighted by the white circle) where the pixels were sampled (Pearson's correlation coefficient $R = 0.78$; Mander's overlap coefficient = 1.0). (E) The intensity of the anti-rac1 (green) and anti-P (red) staining across the infected cell at an optical plane where the inclusion bodies are visualized. Cross-section analysis indicated by white line in (i) and (ii) plotted as an intensity map. Individual inclusion bodies are highlighted (*).

proteins (Lawson and Ridley, 2018). These proteins are activated via a guanidine exchange factor (GEF), and once activated, the rho family of GTPases mediate their effects on the cell cytoskeleton via a variety of downstream effector molecules. The effect that these mediators play in cell signaling is further complicated by “cross-talk” between the different pathways associated with the different rho kinase family members (Hanna and El-Sibai, 2013; Lopez-Posadas et al., 2017).

Inhibiting rhoA activation led to the loss of virus infectivity, and a role for virus-induced rhoA activation in mediating RSV assembly has been demonstrated (Gower et al., 2005; Pастey et al., 2000). Similarly, inhibiting rac1 activation leads to an inhibition of virus particle assembly (Jeffree et al., 2007; Yeo et al., 2009), although it is currently unclear if the rac1 protein plays a direct role in the RSV particle assembly process. In this current investigation we have therefore extended

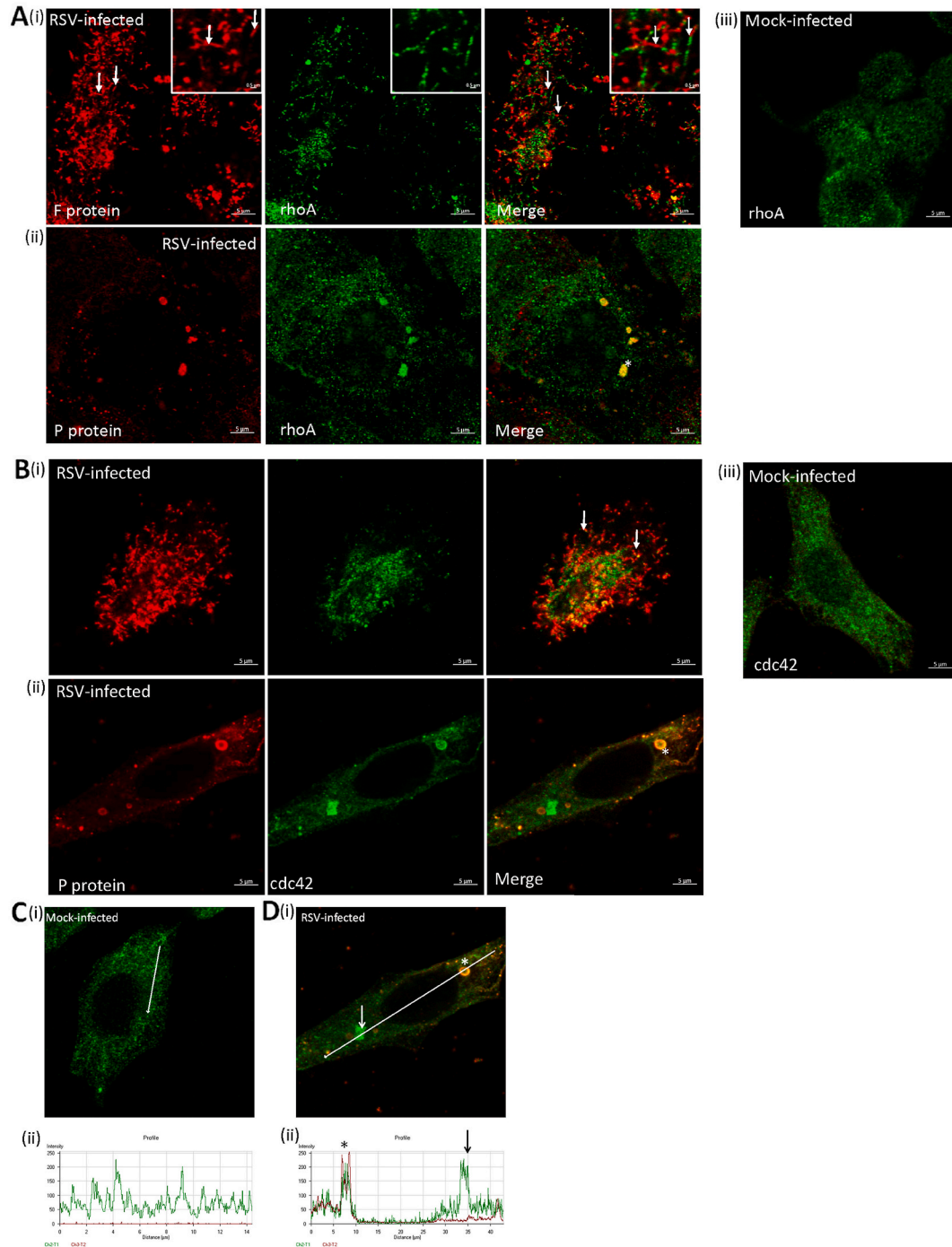


Fig. 2. The distribution of the rhoA and cdc42 proteins in RSV-infected cells. HEp2 cells were RSV-infected and at 18 h post-infection (hpi) the cells were costained with (A) (i) anti-rhoA and anti-F, and (ii) anti-rhoA and anti-P or (B) (i) anti-cdc42 and anti-F and (ii) anti-cdc42 and anti-P. The cells were visualized using confocal microscopy at a focal plane that allowed (i) virus filament detection (highlight by white arrows) and (ii) inclusion body detection (highlighted by *). Also shown are mock-infected cells stained with either anti-rhoA (A) (iii) and anti-cdc42 (B) (iii). The intensity of the anti-cdc42 (green) and anti-P (red) staining in a (C) mock-infected and (D) infected cell at an optical plane where the inclusion bodies were visualized. In each case the cross-section analysis is indicated by white line in (i) and (ii) plotted as an intensity map. An inclusion body (*) and another unspecified type of cdc42 staining pattern detected in infected cells (black arrow) are highlighted.

our earlier observations to better understand the role of the rac1 protein in RSV assembly.

2. Results and discussion

2.1. A sub-population of the rac1 protein cellular pool is associated with virus filaments and inclusion bodies in RSV-infected cells

In this study we have primarily used the HEp2 cell line, since higher levels of virus production occur in HEp2 cells compared with other permissive human cell types commonly used to study RSV infection e.g. A549 cells (Huong et al., 2016). This suggested that HEp2 cells are a suitable cell model system for identifying host cell factors that are required for efficient virus production. In this analysis we used anti-F and anti-G antibodies to detect the presence of virus filaments, anti-P antibody to detect the presence of virus inclusion bodies, and anti-RSV antibody to detect inclusion bodies and virus filaments.

We had previously demonstrated that the activated rac1 protein plays a role in RSV morphogenesis (Yeo et al., 2009), and we hypothesized that if the rac1 protein played a role in RSV particle formation it would be expected to be localized at sites on the cell membrane where virus assembly occurs. Physical connectivity between the virus filaments and inclusion bodies at the surface of virus-infected cells has been demonstrated, suggesting that the inclusion bodies are directly involved in the virus assembly process, and an involvement in the packing of the virus nucleocapsid has been proposed (Jeffree et al., 2007; Radhakrishnan et al., 2010; Santangelo et al., 2006). We would therefore expect to detect the presence of the rac1 protein in both virus filaments and inclusion bodies, and we examined the distribution of the rac1 protein in RSV-infected cells at 18 h post-infection (hpi). Although the focus of this current study was the rac1 protein, activated rhoA protein has also been implicated in RSV assembly and is required for virus filament formation (Gower et al., 2001, 2005). A role for the cdc42 protein in virus entry has been proposed, although no role for the cdc42 protein in virus assembly has been demonstrated. We therefore also compared the distribution of the rac1 protein (Fig. 1) with that of the rhoA and cdc42 proteins (Fig. 2) in RSV-infected cells, since comparing the distribution of the different rhoGTPases in virus-infected cells would allow a greater confidence in assessing the significance of the virus-associated rac1.

RSV-infected cells were co-stained with anti-F (to detect the presence of the virus filaments) or anti-P (to visualise the cytoplasmic inclusion bodies) and anti-rac1 (Fig. 1A). The co-stained cells were then examined using confocal microscopy at a focal plane that allowed detection of virus filaments and inclusion bodies. The anti-F and anti-rac1 co-stained cells exhibited anti-rac1 staining throughout the virus filaments (Fig. 1A(i)), while anti-P and anti-rac1 showed co-staining within the inclusion bodies (Fig. 1A(ii)). The pixel distributions in the images obtained from the co-stained cells were examined which enabled a quantitative analysis of rac1 protein distribution. The high level of co-localizing pixels (indicated by the high Pearson's correlation coefficient and Mander's overlap coefficient), and the correlation of the anti-F and anti-rac1 antibody staining profiles was consistent with the presence of the rac1 protein in virus filaments (Fig. 1B and C) and inclusion bodies (Fig. 1D and E). In anti-F and anti-rhoA co-stained cells the anti-rhoA staining was localized to regions where the anti-F stained-virus filaments appeared, but the anti-rhoA antibody staining appeared localized and was not distributed throughout the virus filaments (Fig. 2A(i)). Co-staining of anti-rhoA in the anti-P stained inclusion bodies was also noted (Fig. 2A(ii)), indicating their association with the inclusion bodies. No co-staining with anti-cdc42 within the virus filaments was indicated (Fig. 2B(i)), although co-staining in the inclusion bodies were again noted (Fig. 2B(ii), C and D). In mock-infected cells a distinct diffuse staining pattern was observed for each of the rho GTPases (Fig. 1A(iii), Fig. 2A(iii) and B(iii)). Although these data indicated presence of the rac1 and rhoA proteins at the site of virus assembly; differences in their distribution on the surface of infected cells was also

noted.

The imaging analysis suggested that a minor proportion of the total cellular pool of the rac1 protein was virus-associated. Since the rac1 protein was detected at the site of virus assembly, we would also expect that this cellular pool of the rac1 protein would be present in a cell-free virus preparation. The cell-free virus particles were isolated from infected cells using discontinuous gradient centrifugation described previously (Radhakrishnan et al., 2010), and examined by immunoblotting using anti-rac1, anti-rhoA and anti-cdc42 (SFig. 1). Two specific fractions were examined in this assay, an infectious virus-containing gradient fraction at the 35–45% sucrose interface (band 1), and a gradient fraction at the 45–60% sucrose interface (band 2) that did not contain infectious virus (SFig. 1A). The immunoblotting analysis indicated the presence of both rac1 and rhoA proteins only in band 1 (SFig. 1B), while the rac1 protein was more readily detected than the rhoA protein. There are caveats when comparing levels of different proteins by immunoblotting using different antibodies, however the greater ease of detection of the rac1 protein suggested a greater abundance of the virus-associated rac1 protein. Although RSV particles co-purified with a variety of different virus-associated host cell factors (Radhakrishnan et al., 2010), collectively the imaging and biochemical analyses are consistent with the presence of the rac1 and rhoA proteins at the site of assembly. The failure to detect the cdc42 protein in the cell-free virus preparation was also consistent with the imaging analysis, and suggested that the cdc42 protein was either not virus filament-associated or it was not efficiently incorporated into the virus filaments i.e. at protein levels below the limit of detection. Although it has recently been proposed that cdc42 may play a role in virus entry (Krzyszaniak et al., 2013), its presence within inclusion bodies suggested that it may play an additional role in the RSV replication cycle.

2.2. RSV infection induces rac1 activation at the site of virus assembly

Previous investigations have demonstrated that RSV infection induced rhoA protein activation, and this was required for virus filament formation (Gower et al., 2001, 2005). Similarly, drugs that selectively inhibited the activity of the rac1 protein also impaired RSV particle assembly, (Jeffree et al., 2007; Yeo et al., 2009), suggesting that the activated rac1 protein was required for virus morphogenesis. However, it remained unclear in our earlier study if this was mediated by a constitutively activated cellular pool of the rac1 protein or if RSV infection induced rac1 protein activation.

Cell lysates were prepared from mock-infected and RSV-infected cells at 18 hpi and examined by immunoblotting with anti-rac1. Similar rac1 protein levels in mock-infected and RSV-infected cells (Fig. 3A) indicated that increased rac1 gene expression did not occur during RSV infection. Cells were either mock-infected or infected with RSV in the absence and presence of the rac1 inhibitor NSC23766, and the activation status of rac1 protein in cell lysates examined at 18 hpi using the established PAK1 pull-down rac1 activation assay (Fig. 3B(i) and (ii)). A low level of activated rac1 protein could be detected in non-infected cells, which is presumably due to low basal levels of constitutively activated rac1 protein required for house-keeping functions in the cell. However, an approximate 7-fold increase in rac1 protein activation levels was detected in RSV-infected cells (Fig. 3B(iii)), indicating that RSV infection induced rac1 protein activation. The NSC23766 inhibits rac1 activation by blocking the interaction of rac1 with its respective GEF (Gao et al., 2004), and a reduced level of the activated rac1 protein in the NSC23766-treated RSV-infected cells was consistent with the inhibition of virus-induced rac1 protein activation. In a parallel analysis we also examined the distribution of the rac1 protein and virus filaments in virus-infected cells at 18 hpi using confocal microscopy. Non-treated and NSC23766-treated virus-infected cells were co-stained using anti-rac1 and anti-F, and examined at a focal plane that allowed detection of virus filaments (Fig. 3C). In non-treated cells we noted the presence of abundant co-stained virus filaments (Fig. 3C(i)), while in

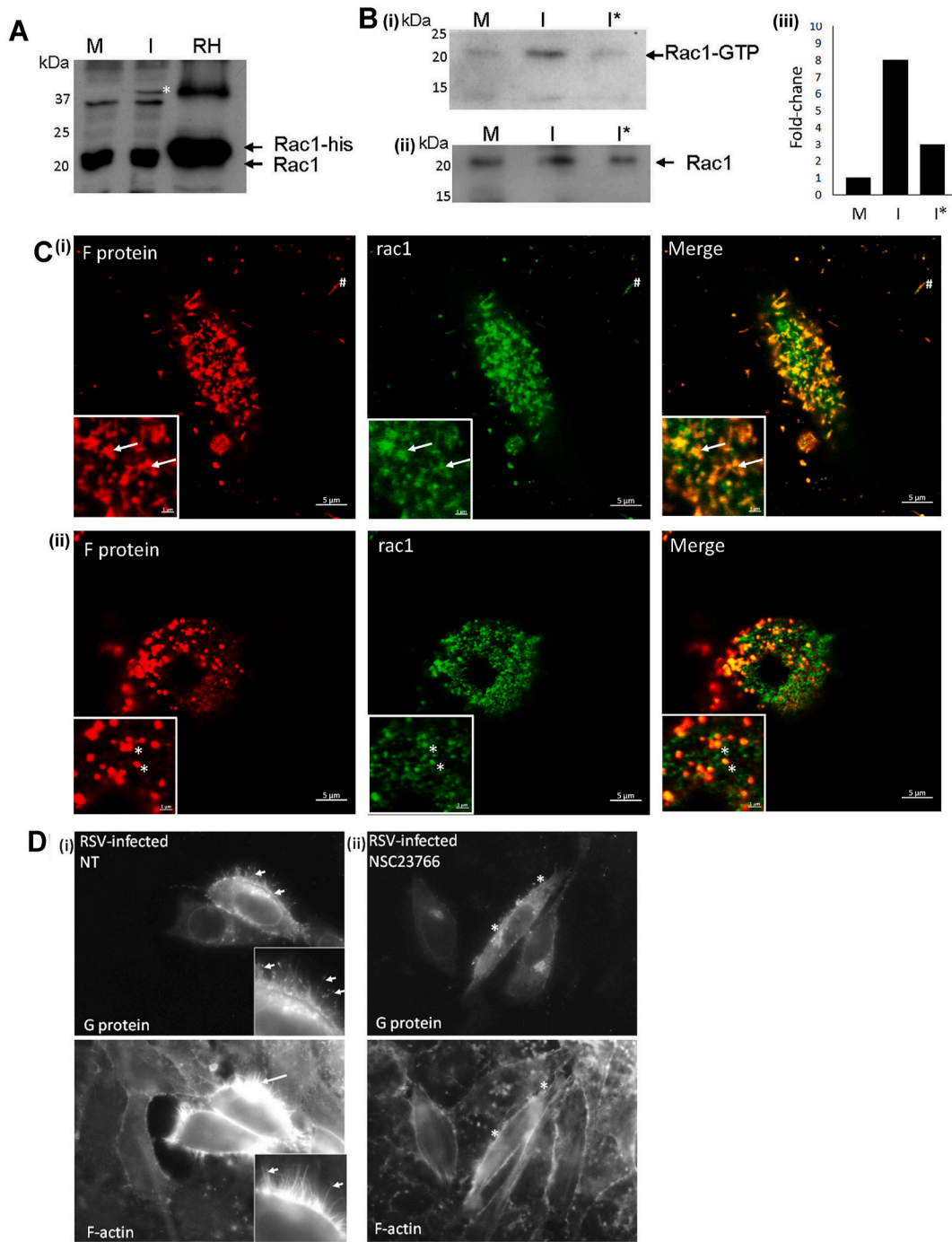


Fig. 3. RSV infection induces activation of the rac1 protein. (A) HEP2 cells were either mock-infected (M) or RSV-infected (I) and at 18 h post-infection (hpi) the presence of the rac1 protein detected in cell lysates by immunoblotting using anti-rac1. The presence of a purified rac1-(6x)his-tagged protein (RH) is also shown for comparison. Also show is a protein species corresponding in size to a rac1 dimer (*) detected in virus-infected cells. (B). HEP2 cells were either mock-infected (M) or RSV-infected in the absence (I) or presence (I*) of NSC23766 and at 18 hpi the lysates were examined (i) for the presence of activated rac1 protein (Rac1-GTP) using the GST-PAK1 pull-down assay. (ii) The total rac1 protein levels in the lysates used to perform the rac-1 activation assay. (iii). Densitometry analysis of the blot in (i) was performed using Image J and the fold-change in intensity with respect to the band detected in mock-infected cells shown. (C) HEP2 cells were RSV-infected in the (i) absence or (ii) presence of NSC23766. At 18 hpi the cells were co-stained with anti-rac1 and anti-F and visualized using confocal microscopy at a focal plane that allowed virus filament detection. The co-stained virus filaments in non-treated cells (white arrows) and punctuate staining pattern in NSC23766-treated cells (*) are highlighted. Inset, in each case an enlarged image is shown from the main plate. (D) HEP2 cells were RSV-infected in the (i) absence (NT) or (ii) presence (NSC23766) of NSC23766 and at 18 hpi the cells were co-stained with anti-G (G protein) and phalloidin-FITC (F-actin). The stained cells were visualized using immunofluorescence microscopy (objective x100 magnification). The anti-G (short arrows) co-stained filamentous projections in the non-treated cells, the staining pattern in drug-treated cells (*), and the phalloidin-FITC staining (long arrows) are highlighted.

NSC23766-treated cells the appearance of an anti-rac1 and anti-F co-stained punctate staining pattern at the cell surface was noted (Fig. 3C(ii)).

In these experiments the NSC23766 was added to virus-infected cells at 5 hpi, which is sufficient time after the initiation of virus infection that the drug would not interfere with virus entry process, but at an early-time point that was prior to the virus filament formation. This was confirmed by imaging RSV-infected cells at between 2 and 18 hpi using anti-G staining (to detect virus filaments) and anti-P staining (to detect inclusion bodies) (SFig. 2). While small anti-P stained inclusion bodies could be detected in some cells at 6 hpi, the anti-G staining only became apparent at 8 hpi (SFig. 2A). Detailed examination of the virus-infected cells at between 12 and 18 hpi using confocal microscopy (SFig. 3A) showed a punctate anti-G staining pattern at 12 hpi, and was consistent with the time of infection prior to virus filament formation. At 14 hpi the appearance of small anti-G stained virus filaments were detected, which increased in size and abundance at between 16 and 18 hpi to produce the morphology-distinct virus filaments (SFig. 3B–D). It has recently been proposed that in infected cells the virus filaments formed at a cellular location below the plasma membrane and migrated to the plasma membrane during virus egress (Vanover et al., 2017). We have not detected virus filaments in the cytoplasm of infected cells by employing electron tomography (Radhakrishnan et al., 2010), however

irrespective of their site of origin in infected cells, our analysis indicated that the addition of NSC23766 at 5 hpi was at a time prior to virus filament formation. The punctuate anti-G staining pattern observed in NSC23766-treated cells at 18 hpi was similar in appearance to the anti-G staining pattern at 12 hpi, suggesting NSC23766 inhibited virus filament formation rather than destabilized the virus filaments after they were formed.

Collectively these data are consistent with a localized activation of the rac1 protein at the site of virus assembly. During RSV morphogenesis changes in the appearance of the cortical F-actin network are consistent with F-actin remodeling (Jeffree et al., 2007; Ravi et al., 2013; Ulloa et al., 1998), and we also examined the effect of NSC23766-treatment on the virus-induced change of the F-actin network (Fig. 3D; SFig. 4A and B). Mock-infected cell monolayers (SFig. 4A(i)), and RSV-infected cell monolayers that were either non-treated (SFig. 4A(ii)) or NSC23766-treated (SFig. 4A(iii)) were co-stained with phalloidin-FITC and anti-G at 18 hpi and examined using IF microscopy. A more detailed analysis of the co-stained non-treated cells infected cells showed the changes in the appearance of the phalloidin-FITC staining pattern that coincided with the formation of virus filaments (Fig. 3D(i); SFig. 4B), and the presence of the virus particles on the F-actin filaments was consistent with a role for F-actin in RSV morphogenesis and transmission. The virus-induced changes in F-actin structure were

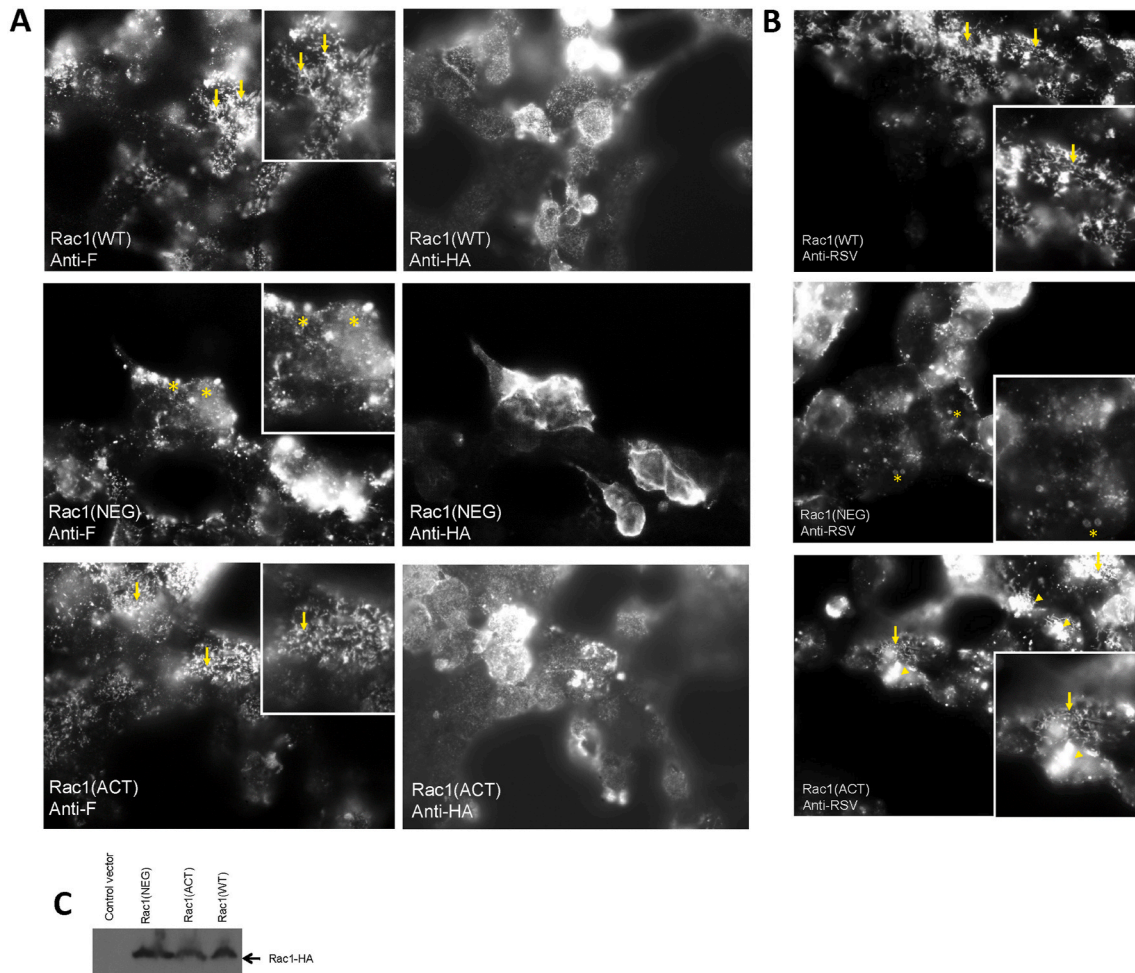


Fig. 4. The dominant negative rac1 phenotype inhibits virus filament formation. (A) HEK cells were transfected with plasmids expressing the wild type HA-rac1 sequence (rac1WT), HA-rac1-G12V (ACT) and HA-rac1-T17N (NEG) and infected with RSV. At 20 h post infection the cells were (A) co-stained using anti-F and anti-HA or (B) anti-RSV and imaged by immunofluorescence microscopy (objective x40 magnification). The virus filaments (arrows), clustered staining pattern (arrow heads) and impaired filaments (*) are highlighted. Insets are enlarged regions taken from the main panel. (C) Immunoblotting of cell lysates from infected cells expressing HA-rac1-T17N, HA-rac1-G12V and HA-rac1 (WT) proteins using anti-HA. Infected cells transfected with pCAGGS (a control vector) and immunoblotted with anti-HA is also shown.

significantly reduced on NSC23766-treated cells (Fig. 3D(ii)), and this coincided with the absence of virus filaments. These data provided evidence that the activated rac1 protein may play a role in the localized F-actin remodeling during virus filament assembly and virus egress. A more detailed analysis using confocal microscopy to image anti-actin and anti-F co-stained RSV-infected cells showed the presence of virus filaments on F-actin structures extending from the cell periphery (SFig. 4C).

We examined the effect of rac1 activation on RSV particle assembly using an established assay that was independent of the use of small molecule rac1 protein inhibitors. This widely used assay has been used to examine the effect of rac1 activation in a variety of different cellular processes by expressing dominant active and inactive forms of the rac1

protein (e.g. (Akedo et al., 2002; Moore et al., 1997)). We examined RSV infection in HEK cells expressing the wild type rac1 protein (rac1WT) and mutant forms of the rac1 protein that were constitutively dominant activated rac1(G12V) protein (rac1ACT) and dominant inactivated rac1(T17N) protein (rac1NEG). The effect of these different rac1 protein forms on RSV assembly was assessed by examining the presence of virus filaments on anti-F (Fig. 4A) and anti-RSV (Fig. 4B) stained cells using IF microscopy. Anti-F and anti-RSV staining was detected in cells expressing each of the different rac1 protein constructs, indicating that these different forms of the rac1 protein did not inhibit the early stages of RSV infection. However, while virus filament formation was observed in cells expressing either the rac1WT or rac1ACT proteins, we failed to detect virus filaments on cells expressing the rac1NEG protein. Each of

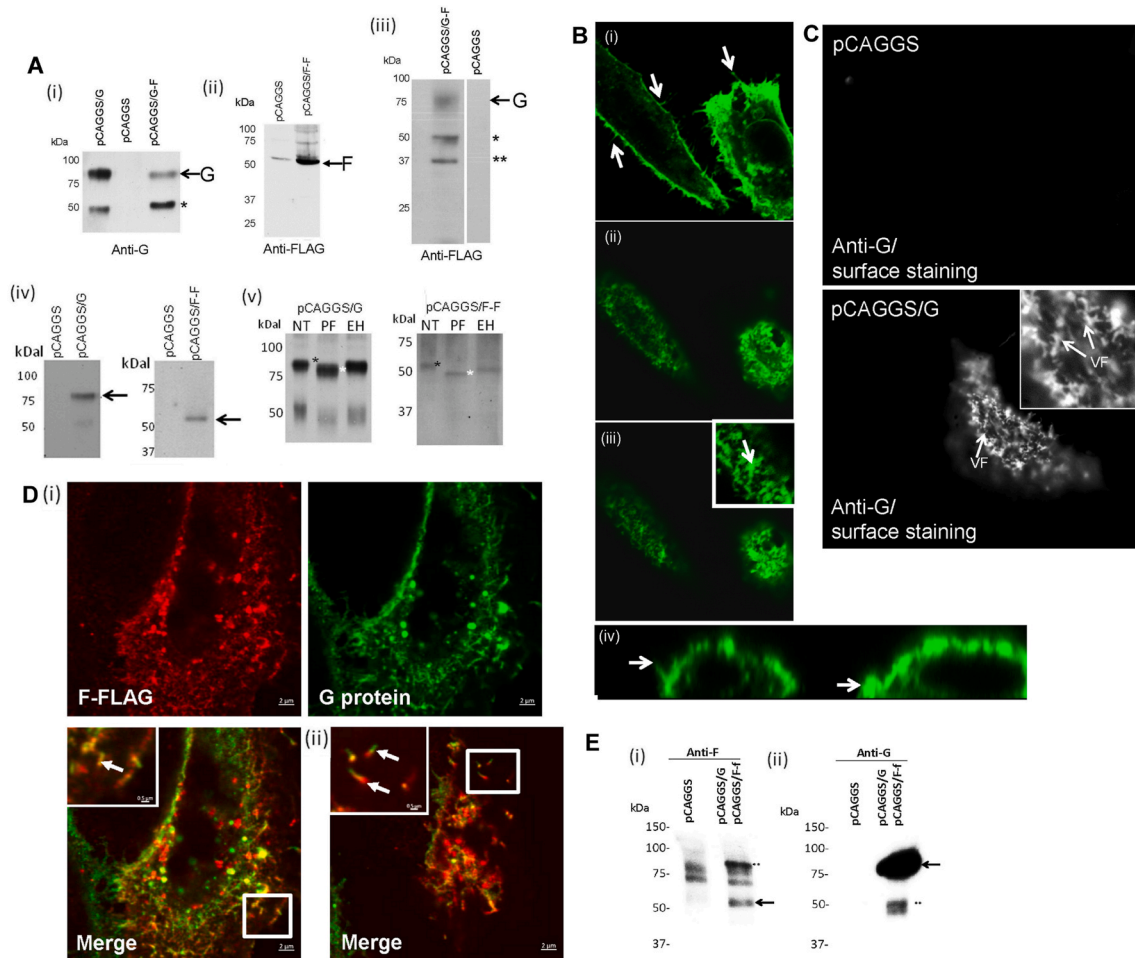


Fig. 5. The recombinant G protein is able to form virus-like particles on HEp2 cells. (A) HEK cells were transfected with (i) pCAGGS, pCAGGS/G and pCAGGS/G-FLAG (G-F), (ii) pCAGGS and pCAGGS/F-FLAG (F-F) and (iii) pCAGGS and pCAGGS/G-FLAG (G-F) and the cell lysates were immunoblotted using anti-G and anti-FLAG as indicated. The location of the specific RSV proteins is highlighted (black arrows). The expected sizes of the nonglycosylated (***) and N-linked glycosylated (*) G proteins are indicated. (iv) Cells were transfected with pCAGGS/G and pCAGGS/F-FLAG (F-F), surface biotinylated, immunoprecipitated with anti-G and anti-F respectively and examined by Western blotting. The mature biotinylated F protein (F1 subunit) and G proteins are indicated (black arrow). Also shown is the same assay conducted in pCAGGS transfected cells. (v) The surface biotinylated G and F (F1 subunit) proteins were immunoprecipitated with anti-F and anti-G respectively and either non-treated (NT), PNGaseF-treated (PF) or endoH-treated (EH) and examined by Western blotting. In each case the N-linked glycosylated (black *) and deglycosylated (white *) proteins are highlighted. (B) HEp2 cells were transfected with pCAGGS/G and stained using anti-G and examined by confocal microscopy at optical planes that allowed imaging of the (i) cell periphery ((ii) cell surface and (iii) the top of the cell.(iv) is a side profile of the transfected cells showing the surface expression of the recombinant G protein. The formation of filamentous projections is highlighted (white arrow). Inset in (iii) is an enlarged image taken from the main panel. (C) HEp2 cells were transfected with either pCAGGS or pCAGGS/G and the non-permeabilised cells stained using anti-G. The cell surface anti-G stained virus protein filamentous structures (VF) are highlighted. Inset is an enlarged image taken from the main plate highlighted (open white box). (D) HEp2 cells were co-transfected with pCAGGS/G and pCAGGS/F-FLAG and co-stained using anti-G and anti-FLAG. The cells were examined by confocal microscopy at optical planes that allowed imaging of the (i) cell periphery and (ii) the top of the cell (only the merged image is shown). The formation of filamentous projections are highlighted (white arrow). In each case the inset is an enlarged image taken from the main plate highlighted (open white box). (E) pCAGGS and pCAGGS/G and pCAGGS/F-FLAG co-transfected HEp2 cells were surface biotinylated and immunoprecipitated with (i) mab19 (anti-F) and (ii) anti-G, and protein species of the expected size for the F1 and G proteins respectively are indicated (black arrow). Additional biotinylated protein species that were immunoprecipitated from the co-transfected cells with anti-F and anti-G (**) are highlighted.

the recombinant rac1 protein forms were expressed with an HA-epitope tag, and immunoblotting of cell lysates prepared from cells expressing each of the rac1 variants with anti-HA demonstrated similar levels of total rac1-HA in each transfection condition (Fig. 4C). These data supported the conclusions using the small molecular inhibitors, that virus-induced rac1 protein activation at the site of virus assembly was required for virus filament formation.

2.3. The recombinant expressed G protein is able to form virus-like particles (VLPs)

Although the rac1 protein was present at the site of virus particle assembly, it was unclear if prior to virus assembly the virus structural proteins were trafficked to locations on the plasma membrane containing the rac1 protein. We partly addressed this question by examining the rac1 protein distribution in non-infected cells expressing virus-like

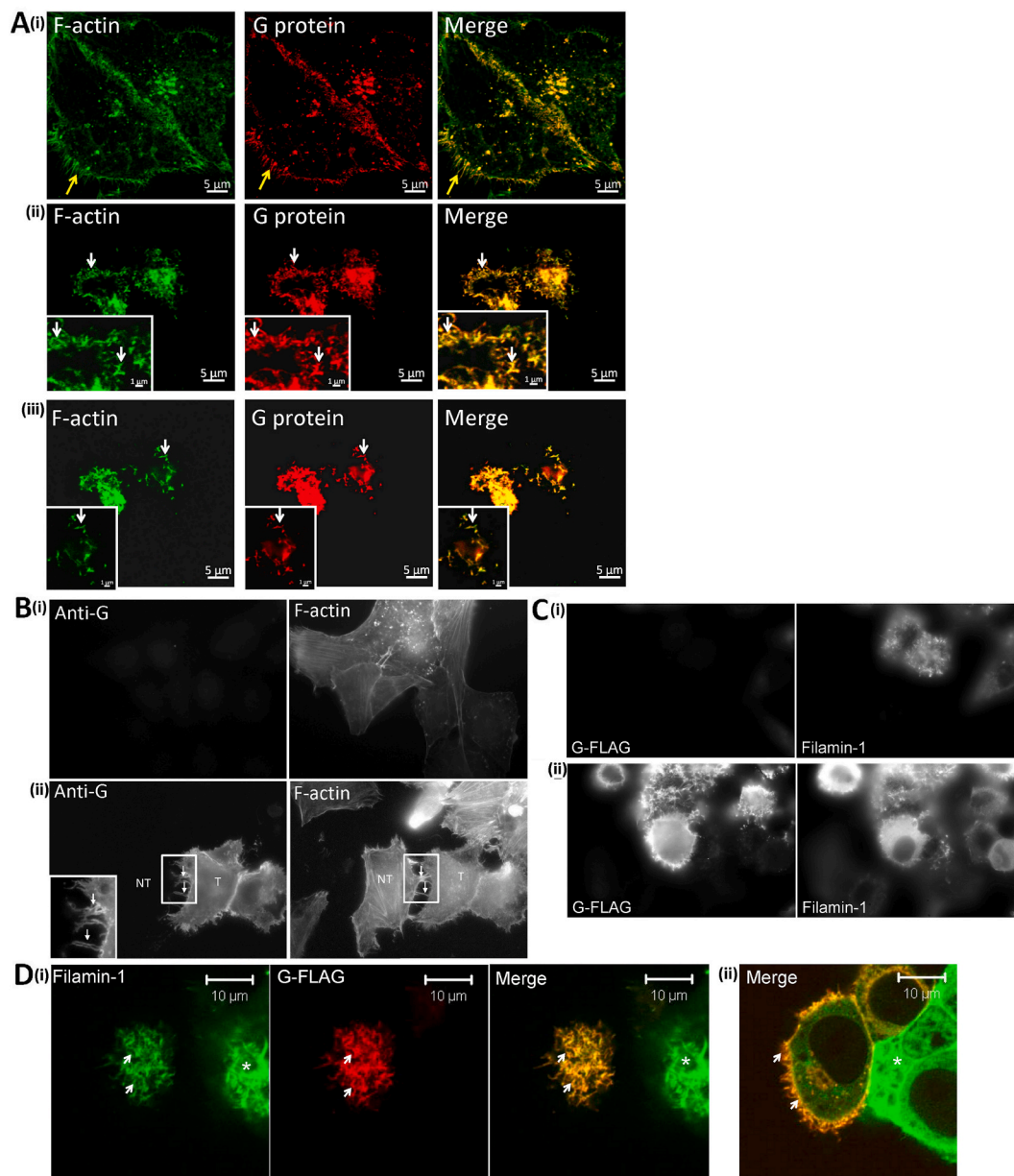


Fig. 6. The recombinant G protein is trafficked into membrane domains containing F-actin and filamin-1. HEP2 cells were transfected with (A) pCAGGS/G and stained using anti-G and phalloidin-FITC. The cells were examined by confocal microscopy at an optical plane that allowed imaging of (i) cell periphery (Pearson's correlation coefficient = 0.89; Mander's overlap coefficient = 1.0) and (ii and iii) cell top (Pearson's correlation coefficient = 0.85; Mander's overlap coefficient = 1.0). The filamentous staining pattern at the cell periphery (yellow arrow) and at the cell top (white arrow) is highlighted. Inset, is an enlarged image taken from the main plate. (B) HEP2 cells were transfected with (i) pCAGGS and (ii) pCAGGS/G and stained with anti-G and phalloidin-FITC (F-actin), and visualized using immunofluorescence microscopy (objective x100 magnification). The transfected (T) and non-transfected (NT) cells and the co-stained filamentous projections extending from transfected to non-transfected cells are highlighted (white arrow). Inset, is an enlarged image taken from the main plate in region highlighted by the open white box. (C) Cells were transfected with (i) pCAGGS or (ii) pCAGGS/G-FLAG and stained using anti-FLAG (G-FLAG) and anti-filamin-1 (Filamin-1). The cells were examined by fluorescence microscopy to allow imaging of cell top (Objective x100 magnification). (D) pCAGGS/G-FLAG transfected cells were stained using anti-FLAG (G-FLAG) and anti-filamin-1 and examined by confocal microscopy at an optical plane that allowed imaging of (i) cell top (Pearson's correlation coefficient = 0.89; Mander's overlap coefficient = 1.0) and (ii) cell periphery (only the merge image is shown). The non-transfected cells (*) and co-stained filamentous structures are highlighted (white arrows).

particles (VLPs). We have previously shown that human metapneumovirus (HMPV) form structures that resembled the virus filaments that formed on infected cells (Jumat et al., 2014), and that the recombinant HMPV G protein was the minimal requirement for the formation of these VLPs (Loo et al., 2013). This earlier study suggested that the HMPV G protein could be used to locate potential sites on the surface of non-infected cells that could be used for HMPV assembly. Due to the

sequence similarity of the RSV and HMPV G proteins we hypothesized that expression of the recombinant RSV G protein in non-infected cells could likewise be used as a marker to visualise the sites of RSV assembly in non-infected cells.

Cell lysates were prepared from cells expressing the recombinant G protein, G-FLAG protein and F-FLAG protein, and immunoblotted with anti-G and anti-FLAG as appropriate (Fig. 5A (i)-(iii)). This revealed

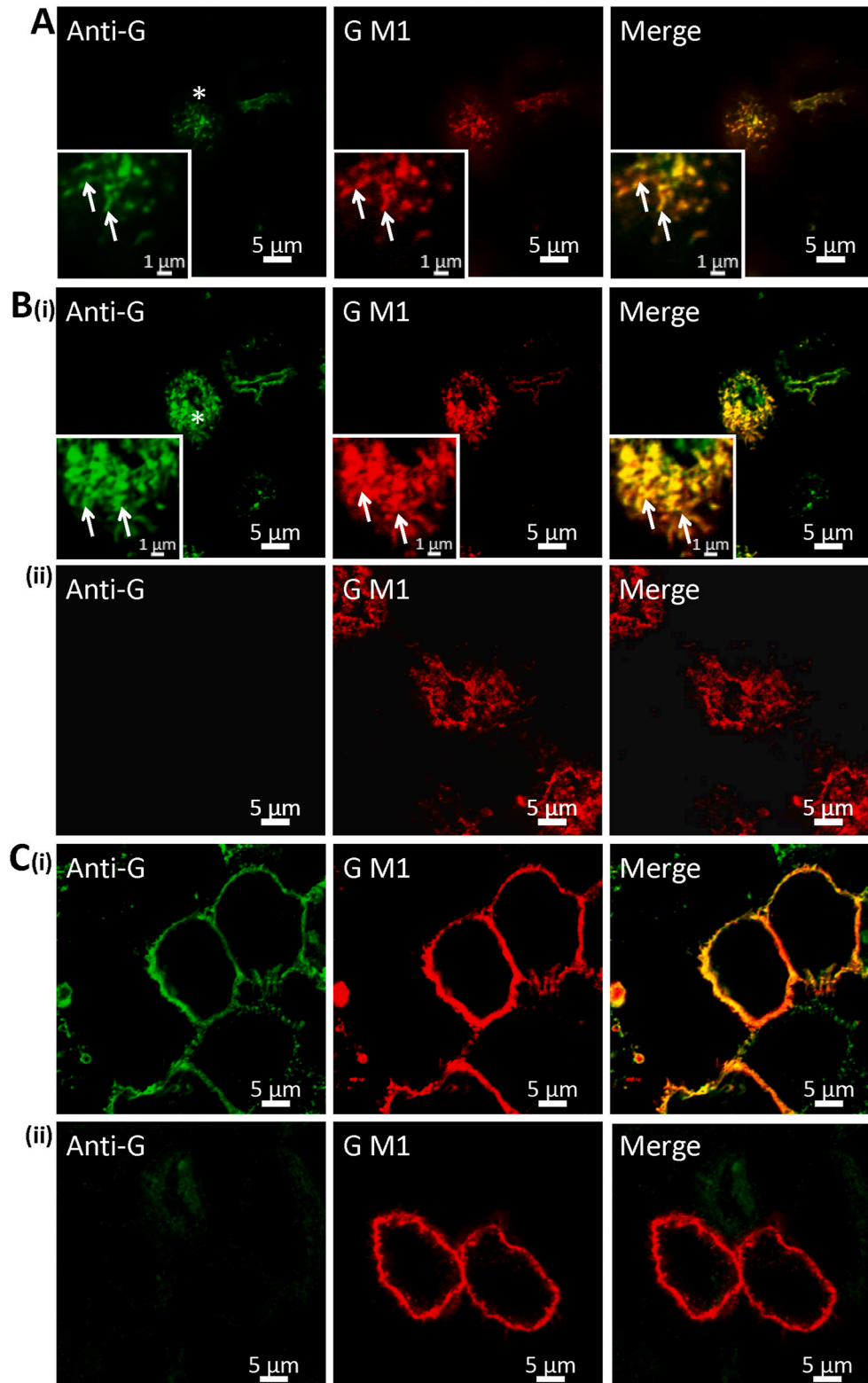


Fig. 7. The recombinant G protein is trafficked to GM1 enriched membrane domains. Cells transfected with pCAGGS/G (A) and (B(i)) and (C(i)) or pCAGGS (B(ii)) and (C(ii)) at stained using anti-G and CTX-B-594 (GM1). The cells were examined by confocal microscopy at an optical plane that allowed imaging of (A and B) cell top ((B)(i) Pearson's correlation coefficient = 0.85; Mander's overlap coefficient = 1.0) and (C) cell periphery. The filamentous co-staining pattern is highlighted (white arrows). Inset is an enlarged image taken in region from the main plate and is highlighted (*).

protein species of the expected size for the F protein (F1 subunit) and G proteins, confirming the expression of the individual recombinant virus proteins. In our hands we noted that expression of the F-FLAG protein enabled higher expression levels of the recombinant expressed F protein compared with the untagged F protein sequence (THP Tan and Sugrue, unpublished observation), and although the reason for this is currently unclear, the FLAG-tagged F protein was used in our experiments. Analysis of the surface expressed F and G proteins by surface-biotinylation confirmed the expression of the mature recombinant F and G proteins at the cell surface (5A (iv)), and the endoglycosidase-H resistance of the surface-expressed recombinant F and G protein confirmed the correct processing of their attached N-linked glycans (Fig. 5A(v)).

The RSV filaments remain largely cell-associated on the surface of infected cells (Huong et al., 2016), and we therefore expected to detect the presence of the RSV VLPs on the surface of transfected cells. HEp2 cells expressing the recombinant G protein were stained with anti-G and then examined using confocal microscopy (Fig. 5B; SFig. 5). In cells expressing the recombinant G protein we observed a prominent filamentous anti-G stained structures at both the cell periphery (Fig. 5B(i)) and at the top of the transfected cells (Fig. 5B(ii) and (iii)), which were similar in appearance to the virus filaments that form on RSV-infected cells. Examination of the anti-G stained transfected cells in cross-section (Fig. 5B(iv)) and non-permeabilized cells confirmed the surface expression of the recombinant G on the transfected cells (Fig. 5C). The appearance of the F protein within the anti-G stained filaments on cells co-expressing the recombinant G and F-FLAG proteins (Fig. 5D (i) and (ii)) was also noted. Although there appeared to be a lower level of F protein expression compared to G protein expression, the incorporation of recombinant F protein into the anti-G stained filaments was consistent with RSV VLP formation. The surface expression of the recombinant G protein and F-FLAG protein in co-transfected cells was confirmed by immunoprecipitation of lysates prepared from surface-biotinylated cells (Fig. 5E), which revealed biotinylated protein species of the expected size of the G and F1 protein's. A 90 kDa protein species that was similar in size to the RSV G protein also co-precipitated with the F1 protein. A similar experimental approach using RSV-infected cells previously demonstrated the interaction between the F and G proteins on the surface of virus infected cells (Low et al., 2008). The appearance of the 90 kDa protein in the immunoprecipitation assay from co-transfected cells suggested that a similar interaction may also occur on the surface of co-transfected cells. These data suggested that expression of the RSV G protein alone was sufficient for VLP formation, and further suggested that in non-infected cells the recombinant RSV G protein could be used as a marker to visualise the cellular location used for RSV assembly. These data were also consistent with the virus glycoproteins playing a direct role in RSV particle assembly (Batonick and Wertz, 2011).

During RSV particle assembly, F-actin and the F-actin-binding protein filamin-1 are incorporated into the virus filaments, providing evidence that these cellular factors are at the site of virus assembly (Brown et al., 2002b; Radhakrishnan et al., 2010). Virus-specific changes in the F-actin staining in virus-infected cells are consistent with virus-induced remodeling of the cell surface during virus filament formation and suggest a role for F-actin particle assembly (Burke et al., 1998; Ravi et al., 2013; Ulloa et al., 1998). Since filamin-1 is also an established F-actin binding protein we also used IF microscopy to examine anti-F and anti-filamin-1 co-stained mock-infected and RSV-infected cells (SFig. 6). While in mock-infected cells the anti-filamin1 staining pattern was similar to that in transfected cells, in virus-infected cells we noted a virus-induced change in the filamin-1 staining pattern that was similar to the change in the F-actin staining observed in RSV-infected cells (Burke et al., 1998; Ravi et al., 2013; Ulloa et al., 1998). These data are also consistent with virus-induced remodeling of the cortical F-actin network at the cell surface during virus filament formation. Since both proteins are associated with virus filaments it would therefore be

expected that these cellular factors would also be present at the locations on the cell surface where the VLPs formed i.e. where the recombinant G protein accumulated. The presence of anti-G and phalloidin-FITC co-stained projections at both the cell periphery (Fig. 6A(i)) and at the cell top (Fig. 6A(ii) and (iii)) was detected using confocal microscopy. The presence of co-stained filamentous structures that extended to neighboring non-transfected cells were also noted (Fig. 6B), and these were similar in appearance to the F-actin connections that extended from RSV-infected cells to non-infected cells during localized cell-to-cell virus transmission (Huong et al., 2016). A similar analysis of cells expressing the G-FLAG protein and stained with anti-filamin-1 showed high levels of anti-FLAG and anti-filamin-1 co-staining in filamentous projections at both cell top (Fig. 6C and D(i)) and at the cell periphery (Fig. 6D(ii)).

Several studies have provided evidence that RSV particle assembly occurs in specialized lipid raft domains (Brown et al., 2002b, 2004; McCurdy and Graham, 2003). Since the accumulation of the raft lipid GM1 at the site of virus assembly is an indicator that RSV assembly occurs in lipid raft microdomains, we also examined the distribution of GM1 in cells expressing the recombinant G protein. In cells expressing the recombinant G protein a high level of anti-G and CTX-B AF555 (to detect GM1) co-staining was observed within the filamentous projections at the cell top (Fig. 7A and B) and at the cell periphery (Fig. 7C). This indicated that the recombinant G protein was trafficked into GM1 enriched microdomains and was consistent with the trafficking of the recombinant G protein into lipid raft microdomains on the cell surface.

Collectively, these data provided evidence that the recombinant G protein was trafficked into lipid-raft microdomains that were stabilized by F-actin and filamin-1. This provided further confidence that the recombinant G protein expressed in non-infected cells could be used to identify sites in the cell that are used for the initiation of RSV particle assembly.

2.4. The *rac1* protein is trafficked to the site of RSV VLP formation

The distribution of the *rac1* protein in HEp2 cells expressing the recombinant G protein and a HA-tagged *rac1* protein (*rac1*-HA) was similarly examined by using confocal microscopy (Fig. 8). The cells were co-stained with anti-G and anti-HA, and distribution of the G protein and *rac1*-HA proteins examined at the cell top (Fig. 8A(i) and (ii)) and cell periphery (Fig. 8A(iii)). Co-staining of both antibodies within the filamentous projections that were formed by the recombinant expressed G protein indicated the presence of the *rac1* protein at the plasma membrane where the recombinant G protein had accumulated. Quantitative analysis of anti-G and anti-*rac1* pixel distribution in the co-stained cells co-expressing the recombinant expressed *rac1* and G proteins was performed at both the cell-base and cell-top. While the quantitative analysis indicated no co-localization between both antibodies at the base of the co-transfected cells (Fig. 8B and C), high levels of co-staining in the filamentous projections on top of the co-transfected cells was confirmed (Fig. 8D and E), and indicated the presence of the *rac1* protein within the VLPs. These data provided evidence that in the absence of infection, the G protein and *rac1* protein were trafficked to the same F-actin-stabilized structures at the plasma membrane.

The incorporation of the virus glycoprotein in the envelope of virus filaments is a prerequisite for the formation of infectious virus particles, and the virus glycoproteins accumulated at the site of RSV assembly (Jeffrey et al., 2003). Our observations demonstrated that the recombinant-expressed virus glycoproteins are trafficked to preexisting F-actin stabilized cellular structures at the cell surface. Filamentous F-actin surface projections are detected on non-infected HEp2 cells but these appeared as relaxed and somewhat flaccid structures when viewed by IF microscopy (Ravi et al., 2013). During the later stages on the virus replication cycle these cellular structures appeared to disappear and be replaced by the virus filaments, which appeared as smaller and more rigid structures when examined by IF microscopy. The anti-G stained VLPs were more similar in appearance to the filamentous projections

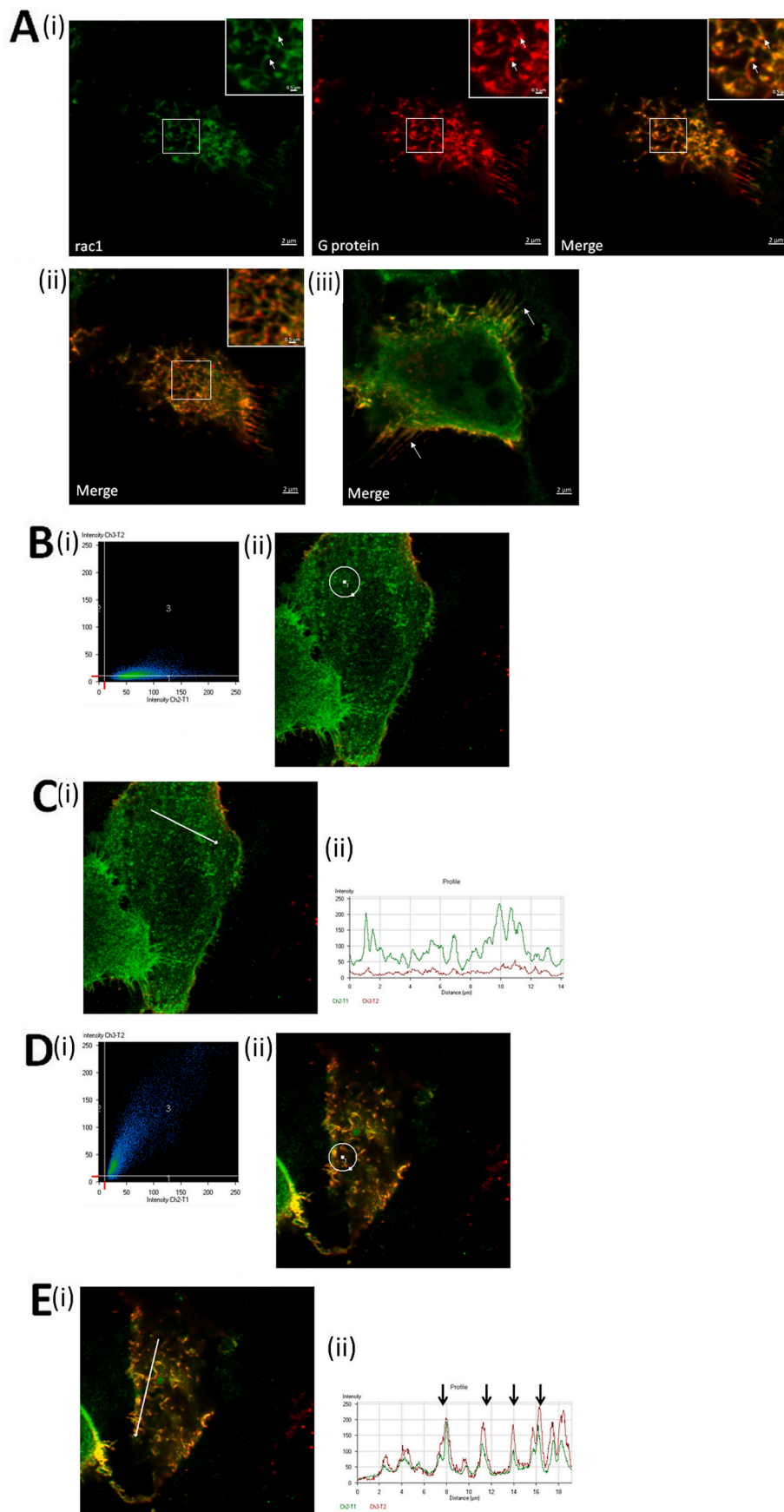


Fig. 8. The recombinant G protein accumulates at cell surface structures containing rac1 protein. HEp2 cells were co-transfected with pCAGGS/G and pXJ-HA-Rac WT and the cells were stained using anti-G and anti-HA. **(A)** The cells were examined in an optical plane that allowed the (i and ii) cell top and (iii) cell periphery to be imaged. Inset is an enlarged image taken from the main plate in region highlighted (open white box). The filamentous co-staining pattern at the cell top (short arrows) and cell periphery (long arrows) are highlighted. Analysis of anti-G and anti-HA staining at **(B and C)** the cell base and **(D and E)** cell top of another representative co-stained cell. **(B and D)** (i) The scatter-plot of the red and green pixels in the anti-rac1 (green) and anti-FLAG (red) co-stained cells in (ii) the area (highlighted by the white circle) where the pixels were sampled. In **D** (i) (Pearson's correlation coefficient $R = 0.88$; Mander's overlap coefficient = 1.0). **(C and E)** The intensity of the anti-rac1 (green) and anti-G (red) staining is shown in a cross-section analysis indicated by white line in (i) and (ii) plotted as an intensity map. The co-stained filaments are highlighted (black arrows).

that are detected on mock-infected cells. We would expect that during the course of RSV infection the activation of specific cellular signaling networks would ultimately mediate additional structural rearrangements at these sites (e.g. via rhoA and rac1 protein signaling). Although a degree of morphological change in the cell surface features where the recombinant expressed G protein was trafficked would be expected, we have thus far failed to detect rac1 activation in cells expressing the recombinant G protein (Jumat and Sugrue; unpublished observations). Although we proposed that the recombinant G protein demarcated the sites of virus assembly, it is unlikely that the filamentous VLPs are morphologically identical to the virus filaments that formed on infected cells. Therefore, while the recombinant G protein would persist at these locations in non-infected transfected cell, in RSV-infected cells these sites would be remodeled by the activation of signaling pathways at the site of assembly prior to virus filament formation. In this context, the virus filaments that form on the infected cells could be regarded as virus-modified cellular structures that are used for the transport of cargo (e.g. the virus genomes) into non-infected cells during localized virus transmission.

3. Conclusion

Under normal physiological conditions, changes in F-actin structure are mediated by rho GTPases as part of larger down-stream signaling cascades (e.g. during cell migration). Many viruses have evolved to use the cellular cytoskeleton at different stages of virus replication cycle, and this is achieved by modulating the signaling pathways that regulate these cell structures (reviewed in (Taylor et al., 2011)). Localized remodeling of the cortical F-actin network during RSV particle formation is proposed to form part of an actin-based motility mechanism that mediates localized virus transmission (Gower et al., 2001, 2005; Jeffree et al., 2007; Ravi et al., 2013; Ulloa et al., 1998). Inhibiting either the rac-1 or rhoA protein activity leads to aberrant particle assembly and reduced virus transmission (Gower and Graham, 2001; Gower et al., 2005; Jeffree et al., 2007; Yeo et al., 2009), indicating that both activities are independently required for particle assembly. This may indicate that the rhoA and rac1 proteins activate two separate and independent down-stream signaling pathways that are required at different stages of the virus assembly process. This would be consistent with the different distributions of the rac1 and rhoA proteins at the site of virus assembly in virus-infected cells. However, since there is cross-talk between the rac1 and rhoA signaling pathways, it is also possible that these two different signaling pathways may converge into a common down-stream pathway that drives the virus assembly process. The inclusion bodies are closely associated with the virus filaments in infected cells, suggesting that they may also play a direct role in the process of virus morphogenesis (Radhakrishnan et al., 2010; Santangelo et al., 2006; Santangelo and Bao, 2007). Both the rhoA and rac1 protein were localized within the inclusion bodies, suggesting that these proteins may also perform signaling functions in the inclusion bodies that may be required for virus morphogenesis.

The rac1 protein plays a central role in several non-infectious human diseases (e.g. Human cancers), and in many cases increased activation of the rac1 protein has been reported in these conditions. The rac1 protein has therefore been identified as a focus with which to directly target using small molecule inhibitors (Cannon et al., 2020; Maldonado et al., 2020), although no FDA-approved therapeutic rac1-specific drugs currently exist. It is currently unclear if the rac1 protein would similarly be a viable drug target to develop antiviral strategies against RSV, and this would require validation in a suitable animal model system. However it is also expected that membrane-association of the rac1 protein would be required for it to mediate its effect during virus particle assembly. Membrane targeting of the rac1 protein by isoprenylation involves the transfer of geranyl-geranyl moieties to the C-terminus of the rac1 protein (Wang and Casey, 2016), and the mevalonate pathway plays a key role in rac1 protein isoprenylation. The enzyme

3-hydroxy-3-methyl-glutaryl-coenzyme A reductase (HMGCR) is a key regulator of mevalonate pathway (Alberts, 1988), and in this context several enzymes in the mevalonate and isoprenoid pathways show upregulated gene expression during the early phase of RSV infection (Ravi et al., 2013; Yeo et al., 2009). Inhibiting HMGCR by lovastatin leads to a general inhibition of protein prenylation in the cell, including rac1 protein prenylation (McTaggart, 2006). Although prenylation of the rac1 protein is not required for its activation (Akula et al., 2019; van der Burgh et al., 2014), prenylation is required for the interaction of the rac1 protein with the plasma membrane where it can exert its biological effect (Kinsella et al., 1991; Molnar et al., 2001). Lovastatin treatment inhibits RSV morphogenesis and localized virus transmission in a cholesterol-independent manner (Gower and Graham, 2001; Ravi et al., 2013), and the role of prenylation in membrane targeting of the rhoA and rac1 proteins may therefore partially provide a molecular basis for this antiviral effect.

Irrespective of the pathways involved, the rac1 protein is likely to exert its effect via one or more down-stream effector molecules. In RSV-infected cells it is currently unclear which downstream rac1-specific effector proteins are involved in the RSV particle assembly process, or even if this effect is mediated via one or more different virus and cellular proteins. Although established down-stream effectors of the rac1 protein have been identified (e.g. PAK1), in RSV-infected cells the rac1 protein may mediate its effect via other, as yet unidentified, cellular proteins. In this context proteomic analysis of isolated virus particles indicates that virus filaments are complex structures that contain additional cellular factors, which include actin and the actin-binding protein filamin-1 (Ludwig et al., 2017; Radhakrishnan et al., 2010). Filamin-1 is an established actin binding protein that can cross-link actin bundles into stable gel-like structures, leading to the formation of modified F-actin structures with unique biological properties (Taylor and Taylor, 1999; Weirich et al., 2017). Since actin and filamin-1 are associated with the virus filaments we can propose that the mature virus particles may also be stabilized by filamin-1-modified F-actin structures. Filamin-1 is also reported to be a ligand for caveolin-1 (Stahlhut and van Deurs, 2000), and both filamin-1 and caveolin-1 are present in virus filaments (Radhakrishnan et al., 2010) and exhibit an altered cell membrane distribution in RSV-infected cells (Ludwig et al., 2017). It is currently unclear if during virus infection caveolin-1 plays a direct role in sequestering filamin-1 into the virus filaments, however the altered distribution of filamin-1 during RSV infection is consistent with RSV-induced F-actin re-modeling (Bitko et al., 2003; Mehedi et al., 2016; Ravi et al., 2013; Ulloa et al., 1998). This suggests that filamin-1 may play a direct role in virus filament formation, and in this context activation of filamin-1 by the rac1 signaling pathway leads to remodeling of the actin cytoskeleton (Bellanger et al., 2000; Ohta et al., 1999; Ramirez-Ramirez et al., 2020; Vadlamudi et al., 2002). It is therefore possible that the activation of the rac1 protein during RSV infection may regulate biological properties of the filamin-1 protein during RSV particle assembly. This may be required for F-actin remodeling and lead to the incorporation of the filamin-1 protein into the virus filaments, a suggestion that is supported by the altered cell membrane distribution of filamin-1 in RSV-infected cells (Ludwig et al., 2017). Future studies will focus on the identification of the down-stream effector proteins that are activated by the rac1 protein during RSV infection, which should allow us a better understanding of the molecular processes that mediate RSV particle assembly.

4. Materials and methods

Cells and virus culture. The RSV A2 strain was propagated and prepared as described previously (Radhakrishnan et al., 2010). The HEp2 and HEK cells were maintained in Dulbecco's Modified Eagle's medium (DMEM) (Invitrogen) supplemented with 10% FCS and 1% penicillin/streptomycin (Invitrogen).

Virus infection. Cell monolayers were infected with RSV using an appropriate multiplicity of infection. Mock-infected and virus-infected

cell monolayers were subsequently maintained in DMEM +2%FCS at 33 °C.

Antibodies and specific reagents. The anti-F antibodies MAb19 and F-Poly were obtained from Geraldine Taylor (Pirbright Institute) and Jose Melero respectively, and the anti-RSV was purchased from Novacastra. The anti-P antibody have been described previously (McDonald et al., 2004; Rixon et al., 2004). The anti-filamin-1 (Santa Cruz), the anti-rac1, anti-rho A and anti-CDC42 (Cytoskeleton, Inc), anti-HA (Sigma), and anti-rabbit and anti-mouse IgG conjugated to Alexa488 and Alexa555 (Invitrogen) were purchased. Phalloidin-FITC (Sigma), phalloidin-Alexa 555 (Invitrogen), cholera toxin-B subunit-Alexa555 (Invitrogen), and NSC23766 (Calbiochem) were purchased. The rac protein expression vectors pXJ-HA-Rac WT, pXJ-HA-Rac V12 and pXJ-HA-Rac N17 were obtained from Dr Koh Cheng Gee (School of Biological Sciences, Nanyang Technological University, Singapore).

Construction of expression vectors. This was performed using standard protocols. Briefly, total RNA was extracted from RSV-infected cells using the RNeasy Kit (Qiagen, Hilden, Germany) and reversed transcribed using SuperScript II RT (Invitrogen). Using the High Fidelity PCR system (Invitrogen), each gene segment was PCR-amplified with gene-specific primers, and the PCR product for each gene was purified using QIAquick Gel Extraction Kit (Qiagen) and cloned into pCR2.1-TOPO or pCR4-TOPO (Invitrogen, Carlsbad, CA, USA) and sequenced. The full-length virus genes were amplified using the High Fidelity PCR system (Invitrogen) using gene-specific primers with suitable restriction enzymes (Stable 1). The C-terminal FLAG-tagged protein sequences were cloned using a reverse primer containing a FLAG-tag sequence. The pCAGGS plasmid and the amplified gene products were digested with their respective restriction enzymes (NEB), ligated using T4 DNA ligase (Roche, Basel, Switzerland), and then transformed into EZ chemical-competent cells (Qiagen). Bulk preparation of individual plasmids was performed using the midiprep kit (Qiagen).

Recombinant protein expression. The transfections were performed using Lipofectamine 2000 (Invitrogen) following the manufacturer's instructions. The transfected cells were maintained at 33 °C until the time of processing.

Transfections of plasmids. The transfections were performed using Lipofectamine 2000 (Invitrogen) following the manufacturer's instructions. The transfected cells were maintained at 33 °C and were processed at 12 h post-transfection.

Immunofluorescence microscopy. Cells on 13 mm glass coverslips were fixed and then stained with the relevant primary and secondary antibodies as described previously (McDonald et al., 2004; Rixon et al., 2004). Unless otherwise specified, the cells were permeabilised using 0.1% Triton X100 in PBS at 4 °C for 15 min prior to antibody staining. The stained cells were mounted on slides using Citifluor and visualized using either a Nikon eclipse 80i fluorescence microscope, or a Zeiss Axioplan 2 LSM510 confocal microscope using appropriate machine settings, and the images examined using Zeiss LSM software.

Cell surface biotinylation analysis. The cell surface biotinylation procedure has been described previously (Sugrue et al., 2001). Briefly, cell monolayers were treated with 500 µg/ml sulfo-NHS-LC-biotin (Pierce) in PBS, pH 8.0, for 30 min at 4 °C. Cell extracts were prepared and immunoprecipitated with either MAb19 or MAb30 at 4 °C and the immune complexes were isolated using protein A-Sepharose for 2 h at 4 °C. After elution in 0.5% SDS, 1% mercaptoethanol (at 100 °C for 10 min), portions of the eluted material were diluted 1:10 in either 50 mM sodium phosphate, 1% NP-40, pH 7.5 or 50 mM sodium citrate, pH 5.5 and incubated at 37 °C for 14 h in the presence of 1000 u PNGase F (NEB) or 1000 u Endo H (NEB) respectively. In non-treated samples the immunoprecipitates were incubated in parallel with 50 mM sodium citrate, pH 5.5 in the absence of enzyme. The biotinylated immunoprecipitates and whole cell lysates were separated by SDS-PAGE and transferred by Western blotting onto PVDF membranes. The PDVF membranes were incubated with streptavidin-HRP and the protein

bands were detected using the ECL protein detection system (Amersham).

Immunoblotting analysis of whole cell extracts. Cells were harvested and washed using PBS (4 °C) and extracted directly into Boiling Mix (final concentration: 1% SDS, 5% mercaptoethanol in 20 mM Tris/HCL, pH 7.5) and heated at 95 °C for 2 min. The cell extracts were clarified by centrifugation (13,000×g for 2 min) and the proteins separated by SDS-PAGE and transferred by Western blotting onto nitrocellulose membranes. In all cases the apparent molecular masses were estimated using Kaleidoscope protein standards (Bio Rad, USA). The protein bands were visualized using the ECL protein detection system (Amersham, USA). The results obtained from the immunoblotting analysis were quantified using ImageJ (ver IJ1.46r). In this case protein bands to be quantified were delineated and the density determined. This was compared with the background intensity in control blank lanes.

Rac1 activity. HEp2 cells were extracted in lysis buffer and the levels of activated rac1 measured using the rac1 pull-down activation assay (Cytoskeleton, Inc). All operations were performed by following the manufacturer's instructions.

CRedit authorship contribution statement

Laxmi Iyer Ravi: Investigation, Data curation. **Timothy J. Tan:** Investigation. **Boon Huan Tan:** Conceptualization, Supervision, Writing – review & editing. **Richard J. Sugrue:** Conceptualization, Writing – original draft, Writing – review & editing, Supervision.

Acknowledgements

We thank National Medical Research Council of Singapore, and National Research Foundation of Singapore for providing funding. Laxmi Iyer Ravi was a recipient of the NTU Post-Graduate Scholarship (Ministry of Education, Singapore). We thank Dr THP Tan, Dr Riahah Jumat, Gaie Brown and Tra Nguyen Huong for technical assistance.

Appendix A. Supplementary data

Supplementary data to this article can be found online at <https://doi.org/10.1016/j.virol.2021.02.008>.

References

- Akeda, Y., Kodama, T., Kashimoto, T., Cantarelli, V., Horiguchi, Y., Nagayama, K., Iida, T., Honda, T., 2002. Dominant-negative Rho, Rac, and Cdc42 facilitate the invasion process of *Vibrio parahaemolyticus* into Caco-2 cells. *Infect. Immun.* 70, 970–973.
- Akula, M.K., Ibrahim, M.X., Ivarsson, E.G., Khan, O.M., Kumar, I.T., Erlandsson, M., Karlsson, C., Xu, X., Brisslert, M., Brakebusch, C., Wang, D., Bokarewa, M., Sayin, V. I., Bergo, M.O., 2019. Protein prenylation restrains innate immunity by inhibiting Rac1 effector interactions. *Nat. Commun.* 10, 3975.
- Alberts, A.W., 1988. Discovery, biochemistry and biology of lovastatin. *Am. J. Cardiol.* 62, 10j–15j.
- Batonick, M., Wertz, G.W., 2011. Requirements for human respiratory syncytial virus glycoproteins in assembly and egress from infected cells. *Adv. Virol.* 2011 <https://doi.org/10.1155/2011/343408>, 2011.
- Bellanger, J.M., Astier, C., Sardet, C., Ohta, Y., Stossel, T.P., Debant, A., 2000. The Rac1 and RhoG-specific GEF domain of Trio targets filamin to remodel cytoskeletal actin. *Nat. Cell Biol.* 2, 888–892.
- Bitko, V., Oldenburg, A., Garmon, N.E., Barik, S., 2003. Profilin is required for viral morphogenesis, syncytium formation, and cell-specific stress fiber induction by respiratory syncytial virus. *BMC Microbiol.* 3, 9.
- Brown, G., Aitken, J., Rixon, H.W., Sugrue, R.J., 2002a. Caveolin-1 is incorporated into mature respiratory syncytial virus particles during virus assembly on the surface of virus-infected cells. *J. General Virol.* 83, 611–621.
- Brown, G., Jeffree, C.E., McDonald, T., Rixon, H.W., Aitken, J.D., Sugrue, R.J., 2004. Analysis of the interaction between respiratory syncytial virus and lipid-rafts in Hep2 cells during infection. *Virology* 327, 175–185.
- Brown, G., Rixon, H.W., Sugrue, R.J., 2002b. Respiratory syncytial virus assembly occurs in GM1-rich regions of the host-cell membrane and alters the cellular distribution of tyrosine phosphorylated caveolin-1. *J. General Virol.* 83, 1841–1850.
- Burke, E., Dupuy, L., Wall, C., Barik, S., 1998. Role of cellular actin in the gene expression and morphogenesis of human respiratory syncytial virus. *Virology* 252, 137–148.

- Cannon, A.C., Uribe-Alvarez, C., Chernoff, J., 2020. RAC1 as a therapeutic target in malignant melanoma. *Trends Canc.* 6, 478–488.
- Carromeu, C., Simabuco, F.M., Tamura, R.E., Fariña Arcieri, L.E., Ventura, A.M., 2007. Intracellular localization of human respiratory syncytial virus L protein. *Arch. Virol.* 152, 2259–2263.
- Collins, P.L., Hill, M.G., Cristina, J., Grosfeld, H., 1996. Transcription elongation factor of respiratory syncytial virus, a nonsegmented negative-strand RNA virus. *Proc. Natl. Acad. Sci. U. S. A.* 93, 81–85.
- Gao, Y., Dickerson, J.B., Guo, F., Zheng, J., Zheng, Y., 2004. Rational design and characterization of a Rac GTPase-specific small molecule inhibitor. *Proc. Natl. Acad. Sci. U.S.A.* 101, 7618–7623.
- García-Beato, R., Melero, J.A., 2000. The C-terminal third of human respiratory syncytial virus attachment (G) protein is partially resistant to protease digestion and is glycosylated in a cell-type-specific manner. *J. Gen. Virol.* 81, 919–927.
- García, J., García-Barreno, B., Vivo, A., Melero, J.A., 1993. Cytoplasmic inclusions of respiratory syncytial virus-infected cells: formation of inclusion bodies in transfected cells that coexpress the nucleoprotein, the phosphoprotein, and the 22K protein. *Virology* 195, 243–247.
- Gower, T.L., Graham, B.S., 2001. Antiviral activity of lovastatin against respiratory syncytial virus in vivo and in vitro. *Antimicrob. Agents Chemother.* 45, 1231–1237.
- Gower, T.L., Pasty, M.K., Peeples, M.E., Collins, P.L., McCurdy, L.H., Hart, T.K., Guth, A., Johnson, T.R., Graham, B.S., 2005. RhoA signaling is required for respiratory syncytial virus-induced syncytium formation and filamentous virion morphology. *J. Virol.* 79, 5326–5336.
- Gower, T.L., Peeples, M.E., Collins, P.L., Graham, B.S., 2001. RhoA is activated during respiratory syncytial virus infection. *Virology* 283, 188–196.
- Grosfeld, H., Hill, M.G., Collins, P.L., 1995. RNA replication by respiratory syncytial virus (RSV) is directed by the N, P, and L proteins; transcription also occurs under these conditions but requires RSV superinfection for efficient synthesis of full-length mRNA. *J. Virol.* 69, 5677–5686.
- Hanna, S., El-Sibai, M., 2013. Signaling networks of Rho GTPases in cell motility. *Cell. Signal.* 25, 1955–1961.
- Huong, T.N., Iyer Ravi, L., Tan, B.H., Sugrue, R.J., 2016. Evidence for a biphasic mode of respiratory syncytial virus transmission in permissive HEp2 cell monolayers. *Virol. J.* 13, 12.
- Jeffrey, C.E., Brown, G., Aitken, J., Su-Yin, D.Y., Tan, B.H., Sugrue, R.J., 2007. Ultrastructural analysis of the interaction between F-actin and respiratory syncytial virus during virus assembly. *Virology* 369, 309–323.
- Jeffrey, C.E., Rixon, H.W., Brown, G., Aitken, J., Sugrue, R.J., 2003. Distribution of the attachment (G) glycoprotein and GM1 within the envelope of mature respiratory syncytial virus filaments revealed using field emission scanning electron microscopy. *Virology* 306, 254–267.
- Jumat, M.R., Nguyen Huong, T., Wong, P., Loo, L.H., Tan, B.H., Fenwick, F., Toms, G.L., Sugrue, R.J., 2014. Imaging analysis of human metapneumovirus-infected cells provides evidence for the involvement of F-actin and the raft-lipid microdomains in virus morphogenesis. *Virol. J.* 11, 198.
- Kallewaard, N.L., Bowen, A.L., Crowe Jr., J.E., 2005. Cooperativity of actin and microtubule elements during replication of respiratory syncytial virus. *Virology* 331, 73–81.
- Kinsella, B.T., Erdman, R.A., Maltese, W.A., 1991. Carboxyl-terminal isoprenylation of ras-related GTP-binding proteins encoded by rac1, rac2, and ralA. *J. Biol. Chem.* 266, 9786–9794.
- Krzyżaniak, M.A., Zumstein, M.T., Gerez, J.A., Picotti, P., Helenius, A., 2013. Host cell entry of respiratory syncytial virus involves macropinosytosis followed by proteolytic activation of the F protein. *PLoS Pathog.* 9, e1003309.
- Lawson, C.D., Ridley, A.J., 2018. Rho GTPase signaling complexes in cell migration and invasion. *J. Cell Biol.* 217, 447–457.
- Leser, G.P., Lamb, R.A., 2017. Lateral organization of influenza virus proteins in the budzone region of the plasma membrane. *J. Virol.* 91.
- Levine, S., Klaiber-Franco, R., Paradiso, P.R., 1987. Demonstration that glycoprotein G is the attachment protein of respiratory syncytial virus. *J. Gen. Virol.* 68 (Pt 9), 2521–2524.
- Loo, L.H., Jumat, M.R., Fu, Y., Ayi, T.C., Wong, P.S., Tee, N.W., Tan, B.H., Sugrue, R.J., 2013. Evidence for the interaction of the human metapneumovirus G and F proteins during virus-like particle formation. *Virol. J.* 10, 294.
- Lopez-Posadas, R., Sturzl, M., Atreya, I., Neurath, M.F., Britzen-Laurent, N., 2017. Interplay of GTPases and cytoskeleton in cellular barrier defects during gut inflammation. *Front. Immunol.* 8, 1240.
- Low, K.W., Tan, T., Ng, K., Tan, B.H., Sugrue, R.J., 2008. The RSV F and G glycoproteins interact to form a complex on the surface of infected cells. *Biochem. Biophys. Res. Commun.* 366, 308–313.
- Ludwig, A., Nguyen, T.H., Leong, D., Ravi, L.I., Huan, T.B., Sandin, S., Sugrue, R.J., 2017. Caveolae provide a specialized membrane environment for respiratory syncytial virus assembly. *J. Cell Sci.* 130, 1037–1050.
- Maldonado, M.D.M., Medina, J.J., Velazquez, L., Dharmawardhane, S., 2020. Targeting rac and Cdc42 GEFs in metastatic cancer. *Front. Cell Dev. Biol.* 8, 201.
- McCurdy, L.H., Graham, B.S., 2003. Role of plasma membrane lipid microdomains in respiratory syncytial virus filament formation. *J. Virol.* 77, 1747–1756.
- McDonald, T.P., Pitt, A.R., Brown, G., Rixon, H.W., Sugrue, R.J., 2004. Evidence that the respiratory syncytial virus polymerase complex associates with lipid rafts in virus-infected cells: a proteomic analysis. *Virology* 330, 147–157.
- McTaggart, S.J., 2006. Isoprenylated proteins. *Cell. Mol. Life Sci.* : CMLS 63, 255–267.
- Mehedi, M., McCarty, T., Martin, S.E., Le Nouën, C., Buehler, E., Chen, Y.C., Smelkinson, M., Ganesan, S., Fischer, E.R., Brock, L.G., Liang, B., Munir, S., Collins, P.L., Buchholz, U.J., 2016. Actin-Related protein 2 (ARP2) and virus-induced filopodia facilitate human respiratory syncytial virus spread. *PLoS Pathog.* 12, e1006062.
- Molnar, G., Dagher, M.C., Geiszt, M., Settleman, J., Ligeti, E., 2001. Role of prenylation in the interaction of Rho-family small GTPases with GTPase activating proteins. *Biochemistry* 40, 10542–10549.
- Moore, K.A., Sethi, R., Doanes, A.M., Johnson, T.M., Pracyk, J.B., Kirby, M., Irani, K., Goldschmidt-Clermont, P.J., Finkel, T., 1997. Rac1 is required for cell proliferation and G2/M progression. *Biochem. J.* 326 (Pt 1), 17–20.
- Ohta, Y., Suzuki, N., Nakamura, S., Hartwig, J.H., Stosel, T.P., 1999. The small GTPase RalA targets filamin to induce filopodia. *Proc. Natl. Acad. Sci. U.S.A.* 96, 2122–2128.
- Pasty, M.K., Gower, T.L., Spearman, P.W., Crowe Jr., J.E., Graham, B.S., 2000. A RhoA-derived peptide inhibits syncytium formation induced by respiratory syncytial virus and parainfluenza virus type 3. *Nat. Med.* 6, 35–40.
- Radhakrishnan, A., Yeo, D., Brown, G., Myaing, M.Z., Iyer, L.R., Fleck, R., Tan, B.H., Aitken, J., Sanmud, D., Tang, K., Yarwood, A., Brink, J., Sugrue, R.J., 2010. Protein analysis of purified respiratory syncytial virus particles reveals an important role for heat shock protein 90 in virus particle assembly. *Mol. Cell. Proteomics : MCP* 9, 1829–1848.
- Ramirez-Ramirez, D., Salgado-Lucio, M.L., Roa-Espitia, A.L., Fierro, R., Gonzalez-Marquez, H., Cordero-Martinez, J., Hernandez-Gonzalez, E.O., 2020. Rac1 is necessary for capacitation and acrosome reaction in Guinea pig spermatozoa. *J. Cell. Biochem.* 121, 2864–2876.
- Ravi, L.I., Liang, L., Wong, P.S., Brown, G., Tan, B.H., Sugrue, R.J., 2013. Increased hydroxymethylglutaryl coenzyme A reductase activity during respiratory syncytial virus infection mediates actin dependent inter-cellular virus transmission. *Antivir. Res.* 100, 259–268.
- Rixon, H.W.M., Brown, G., Aitken, J., McDonald, T., Graham, S., Sugrue, R.J., 2004. The small hydrophobic (SH) protein accumulates within lipid-raft structures of the Golgi complex during respiratory syncytial virus infection. *J. Gen. Virol.* 85, 1153–1165.
- Roberts, S.R., Campans, R.W., Wertz, G.W., 1995. Respiratory syncytial virus matures at the apical surfaces of polarized epithelial cells. *J. Virol.* 69, 2667–2673.
- Santangelo, P., Nitin, N., LaConte, L., Woolums, A., Bao, G., 2006. Live-cell characterization and analysis of a clinical isolate of bovine respiratory syncytial virus, using molecular beacons. *J. Virol.* 80, 682–688.
- Santangelo, P.J., Bao, G., 2007. Dynamics of filamentous viral RNPs prior to egress. *Nucleic Acids Res.* 35, 3602–3611.
- Schmitt, A.P., Lamb, R.A., 2005. Influenza virus assembly and budding at the viral budzone. *Adv. Virus Res.* 64, 383–416.
- Stahlhut, M., van Deurs, B., 2000. Identification of filamin as a novel ligand for caveolin-1: evidence for the organization of caveolin-1-associated membrane domains by the actin cytoskeleton. *Mol. Biol. Cell* 11, 325–337.
- Sugrue, R.J., Brown, C., Brown, G., Aitken, J., Mc, L.R.H.W., 2001. Furin cleavage of the respiratory syncytial virus fusion protein is not a requirement for its transport to the surface of virus-infected cells. *J. General Virol.* 82, 1375–1386.
- Taylor, K.A., Taylor, D.W., 1999. Structural studies of cytoskeletal protein arrays formed on lipid monolayers. *J. Struct. Biol.* 128, 75–81.
- Taylor, M.P., Koyuncu, O.O., Enquist, L.W., 2011. Subversion of the actin cytoskeleton during viral infection. *Nat. Rev. Microbiol.* 9, 427–439.
- Ulloa, L., Serra, R., Asenjo, A., Villanueva, N., 1998. Interactions between cellular actin and human respiratory syncytial virus (HRSV). *Virus Res.* 53, 13–25.
- Vadlamudi, R.K., Li, F., Adam, L., Nguyen, D., Ohta, Y., Stosel, T.P., Kumar, R., 2002. Filamin is essential in actin cytoskeletal assembly mediated by p21-activated kinase 1. *Nat. Cell Biol.* 4, 681–690.
- van der Burgh, R., Pervolaraki, K., Turkenburg, M., Waterham, H.R., Frenkel, J., Boes, M., 2014. Unprenylated RhoA contributes to IL-1β hypersecretion in mevalonate kinase deficiency model through stimulation of Rac1 activity. *J. Biol. Chem.* 289, 27757–27765.
- Vanover, D., Smith, D.V., Blanchard, E.L., Alonas, E., Kirschman, J.L., Lifland, A.W., Zurla, C., Santangelo, P.J., 2017. RSV glycoprotein and genomic RNA dynamics reveal filament assembly prior to the plasma membrane. *Nat. Commun.* 8, 667.
- Wang, M., Casey, P.J., 2016. Protein prenylation: unique fats make their mark on biology. *Nat. Rev. Mol. Cell Biol.* 17, 110–122.
- Weirich, K.L., Banerjee, S., Dasbiswas, K., Witten, T.A., Vaikuntanathan, S., Gardel, M.L., 2017. Liquid behavior of cross-linked actin bundles. *Proc. Natl. Acad. Sci. U.S.A.* 114, 2131–2136.
- Yeo, D.S., Chan, R., Brown, G., Ying, L., Sutejo, R., Aitken, J., Tan, B.H., Wenk, M.R., Sugrue, R.J., 2009. Evidence that selective changes in the lipid composition of raft membranes occur during respiratory syncytial virus infection. *Virology* 386, 168–182.
- Yu, Q., Hardy, R.W., Wertz, G.W., 1995. Functional cDNA clones of the human respiratory syncytial (RS) virus N, P, and L proteins support replication of RS virus genomic RNA analogs and define minimal trans-acting requirements for RNA replication. *J. Virol.* 69, 2412–2419.